JCTC Journal of Chemical Theory and Computation

ARTICLE

pubs.acs.org/JCTC

The Ethidium−UA/AU Intercalation Site: Effect of Model Fragmentation and Backbone Charge State

Karol M. Langner,[†,‡] Tomasz Janowski,[§] Robert W. Góra,[∥] Paweł Dziekoński,[⊥] W. Andrzej Sokalski,[*,†] and Peter Pulay[§]

[†]Institute of Physical and Theoretical Chemistry, Wrocław University of Technology, Wyb. Wyspiańskiego 27, 50-370 Wrocław, Poland

[‡]Leiden Institute of Chemistry, Leiden University, Einsteinweg 55, 2333 CC Leiden, The Netherlands

[§]Department of Chemistry and Biochemistry, Fulbright College of Arts and Sciences, University of Arkansas, Fayetteville, Arkansas 72701, United States

[∥]Theoretical Chemistry Group, Institute of Physical and Theoretical Chemistry, Wrocław University of Technology, Wyb. Wyspiańskiego 27, 50-370 Wrocław, Poland

[⊥]Wrocław Center for Networking and Supercomputing, Wyb. Wyspiańskiego 27, 50-370 Wrocław, Poland

Supporting Information

ABSTRACT: We report a systematic analysis of the intermolecular interactions of cationic ethidium intercalated into a UA/AU step of RNA for a single conformation based on crystallographic coordinates. Interaction energies at the MP2/6-31G** level were partitioned into electrostatic, exchange, delocalization, and correlation components. Various pairwise interaction models built from chemically intuitive fragments reproduce within a few percent values obtained when treating the intercalation site as a whole. Gas phase results are very sensitive to the charge state of the two phosphate groups, with the electrostatic term nearly tripling when the counterions are removed. But this is largely compensated by solvation, an effect represented here within the polarizable continuum model. In a few cases, more diffuse and larger basis sets as well as QCISD(T) corrections were applied in an effort to estimate plausible ethidium-nucleobase electron correlation effects.

1. INTRODUCTION

Since the earliest experimental reports by Lerman and Waring,[1,2] intercalation has been defined by how it affects double helix structure: nucleic acid strands extend and unwind in order to accommodate aromatic ligands between base pairs. Alongside other modes by which small molecules reversibly attach to nucleic acids, such as groove binding and peripheral electrostatic interactions,[3] intercalation is characterized by the parallel alignment of a small aromatic between nucleic acid base pairs. And while disrupting cellular metabolism is their most widely utilized property, the potency of intercalating ligands is now attributed to the inhibition of DNA-binding enzymes such as topoisomerases rather than intercalative binding itself.[4] Nonetheless, the specific type of stacking interaction involved makes these ligands interesting in other ways, for example, as fluorescent probes[5] and switchable ligands.[6] The trademark binding mode of intercalators is even hypothesized to be rooted in an evolutionary role, such as promoting oligonucleotide polymerization during the prebiotic RNA world.[7]

It is clear that in all of these areas the interactions of intercalating molecules with the nearest fragments of their hosts are important. What is still not clear today, however, is how these interactions relate to the process of inserting a ligand into a nucleic acid strand, the molecular basis of which is just starting to be studied.[8] Thermodynamic data concerning intercalation are quite abundant, and generally speaking the stabilizing effect of desolvation and intermolecular interactions balance unfavorable entropic contributions to intercalation arising from conformational changes in the nucleic acid chain and from lost degrees of freedom.[9−11] Such compensation can be used to differentiate between intercalation and groove binding, even if the binding energy is similar.[12] Unfortunately, this compensation also complicates the interpretation of experimental data, since the measured binding free energy is several times smaller than any of the single contributions it is typically divided into.

Here, we turn to the already mentioned local intermolecular interactions, denoted by ΔG_{mol} following Graves and Valea,[10] interactions which in line with Lerman's original interpretation include $\pi-\pi$ aromatic stacking between the intercalator's chromophore and nearest nucleic acid bases. Although various computational methods have been applied to study intercalation complexes already in the previous century,[13−17] works that probe their quantum chemical nature have appeared only in the past decade. This is due to the sizes of the systems involved and also due to the recognized importance of dispersion forces (interactions between instantaneous electron density moments), prohibiting the use of standard density functional theory.

Probably the first to venture in the direction of *ab initio* chemical calculations were Bondarev et al.,[18] who calculated second order Møller−Plesset (MP2) interaction energies separately between the intercalator amiloride and the four DNA bases using the 6-31++G(d,p) basis set. Soon afterward, Řeha et al.[19] followed with a similar, more extensive investigation of four

Received: February 18, 2011
Published: June 18, 2011

intercalators, among them ethidium. The main conclusion of these first reports was that in electronic structure calculations of this kind it is indispensable to account for dispersion effects, as they constitute a substantial part of the interaction energy similarly to conventional stacks of nucleic acid bases.[20] More recently, Kubař et al.[21] have combined molecular dynamics with quantum chemical calculations to estimate the various free energy terms involved in, among other things, a variant of the system studied here (their system comprised ethidium intercalated into a TA/AT step of DNA). They achieved a net binding free energy of −4.5 kcal/mol, close to the corresponding experimental value of −7 kcal/mol, with a stabilization energy component of −70 kcal/mol. This disparity of an order of magnitude again underscores the fact that various free energy contributions are compensated, and that intermolecular stabilization effectively plays a decisive role.

More MP2 calculations have followed, also by Langner et al.,[22] for the same ethidium−UA/AU complex studied here, wherein they focused on the role of the first-order electrostatic component of the interaction energy, and on the horizontal alignment of the intercalator between base pairs. Dračinsky and Castaño[23] performed a similar study earlier, of the interaction energy between ellipticine and base pairs for various distances and twists. Single point energies have also been published by Xiao and Cushman[24] for camptothecin in an attempt to correlate them with experimental site selectivity in ternary cleavage complexes. Due to problems with the proper representation of dispersion interactions by the standard exchange-correlation functionals, density functional theory (DFT) has been adopted relatively late.[25] Time-dependent DFT and Car−Parrinello dynamics have also been employed, for example, by Fantacci et al.,[26] in order to characterize the influence of base pairs on the excited states of an intercalated ruthenium compound.

The MP2 method, despite being the method of choice for sizable systems that include $\pi-\pi$ contacts, is also problematic as far as dispersion forces are concerned. It has been pointed out that it overestimates their magnitude significantly compared to CCSD(T) values,[27] and recently some effort has gone into correcting for this. In the context of nucleic acid intercalation, Hill and Platts[28] have applied local correlation methods and density fitting for several intercalators together with four surrounding nucleobases.

Another problem concerning $\pi-\pi$ stacking interactions is that the dispersion energy saturates slowly with growing Gaussian basis sets. A practical measure applied in many previous studies has been to make polarization functions of small basis sets more diffuse by decreasing their exponents. For example, decreasing the exponent of *d* functions on heavy atoms from 0.8 to 0.25 in the 6-31G* basis set brings interaction energies for stacked nucleic acid bases closer to results obtained in a more saturated basis sets,[29,30] and this protocol has already been used for studying intercalation complexes.[19,21,23]

The focus in almost all of these studies has been on interactions between intercalators and nucleobases. While little has been written about the remaining parts of the nucleic acid strand and the physical nature of their interactions with intercalators, they must also play a role and lately have been garnering increased interest. For example, Horowitz et al.[31] have been the first to compare the NMR structures of intercalated RNA linked at its 2′,5′ ends and previously known 3′,5′-linked RNA intercalation geometries. They showed that while a modified backbone conformation does not change the characteristics of intercalation binding (the unwinding angle and helical rise), it does influence the enthalpic part of the free binding energy. This result hints that intermolecular interactions within the intercalation site are affected by changes in nucleic acid backbone structure, and certainly also by the surroundings.

When they are included in *ab initio* calculations, the phosphate groups are normally capped with protons to simulate the proximity of counterions.[21] Meanwhile, it is known that the behavior of counterions around nucleic acids is not trivial, with monovalent cations being highly diffusive[32] and divalent ions binding more tightly.[33] Definitely in the native, dynamic environment of nucleic acids one would expect significant variations in the hydration shell and counterion positions and therefore also in the electron distribution around phosphate groups.

Geometry fluctuations are definitely also important for noncovalent interactions in intercalator binding sites, a point demonstrated by Svozil et al.[34] for dinucleotides in the gas phase. They find significant variability in stacking interaction energies along molecular dynamics trajectories, and the same may be true for intercalation complexes such as the one studied here. Molecular dynamics calculations suggest[35] that nucleic acid configurational entropy can change considerably upon intercalation, affecting the phosphate groups the most and depending strongly on the host sequence. It would be best to follow these examples and take multiple MD snapshots as input for subsequent interaction energy calculations, but such a systematic treatment is beyond the reach of current computational resources.

We take a first step by considering the various charge states of the phosphate groups. To this end, single point gas phase calculations were performed for ethidium intercalated into a AU/UA base pair step of RNA, in which the phosphate groups were protonated (capped with protons), quenched with counterions, hydrated with single water molecules, or simply left anionic. This selection of charge states gives an idea of the range of possible interaction energies (neglecting conformation effects). Further polarizable continuum calculations roughly correct these values for the more physiologically relevant setting of water solvent.

Another aim here is to probe the validity of dividing intercalation sites into nucleobases and other fragments within the minimal model proposed by Kubař et al.,[21] which consists of the intercalator, four nearest nucleosides, and two phosphate groups between them. We also compare several theoretical approximations and interaction energy components, calculated between ethidium and the RNA fragment as a whole, with selected pairwise interaction schemes. Besides additivity and polarization effects, in this way, we gain information about the relative importance and independence of the molecular fragments within the intercalation site. Finally, a reasonable magnitude for the dispersion interaction is sought by evaluating QCISD(T) energies (quadratic configuration interaction including unlinked triples)[36] and using larger basis sets for the most sensitive part of the system, i.e., the $\pi-\pi$ stacking interaction of ethidium with nucleobases.

2. COMPUTATIONAL METHODS

Despite recent advances and increasingly accurate quantum chemical descriptions of unprecedentedly large molecules,[37,38] including aromatic stacking complexes,[30,39−44] almost all systems relevant to biological processes are still simply too large to be treated *en masse* from first principles routinely. Studies of intercalated nucleic acids have been typically limited to two or four nearby nucleobases, and interactions are usually analyzed

pairwise between the intercalator and each base separately. This seemingly straightforward way to proceed, that is, to divide a system into smaller parts that are as chemically independent as possible, is also the conceptual starting point for many fragmentation strategies such as effective fragment potentials,[44] local correlation approaches,[45] the fragment molecular orbital (FMO) method,[46] and density fitting methods.[28,47,48]

As already mentioned, here, we revisit the ethidium cation intercalated between AU/UA base pairs in a conformation obtained from the crystallography literature.[49] The system will be referred to shortly as $Eth^{(+1)}$—UA/AU throughout this report. In a previous study of the same complex,[22] the ethidium cation was fragmented into its chromophore, ring, and side chain, and interactions with only the four nearest nucleobases were taken into account in a pairwise fashion—in the present work, such an approach defines one of the models used, namely, **A4** (parts). In the previous report, interactions at the MP2 level between the ethidium chromophore and nearest four bases were shown to be sufficient in order to reproduce with crystallographic accuracy the alignment of the intercalator in the intercalation plane. This was repeated there, albeit with limited success, using electrostatic interactions based on atomic multipole moments.

In order to be consistent with previous results, the 6-31G** basis set was also used in this study, unless stated otherwise. For all of the models considered, the interaction energy between ethidium and the intercalation site was decomposed into several terms with generally understood physical meaning according to a hybrid variation—perturbation scheme,[50] and all calculations were done consistently in the dimer-centered basis set following the prescription of Boys and Bernardi.[51]

In a few cases, higher order correlation effects were evaluated by employing additional QCISD(T) calculations and larger basis sets. Only results for the aug-cc-pVDZ basis set (for all methods) are presented here, but several additional MP2 results can be found in the Supporting Information. It is appropriate to comment on our choice of the higher level method (QCI)—the major reason being that the program used[52] is more efficient for QCISD than CCSD. On the other hand, it has been demonstrated that the quadratic corrections satisfactorily account for size-consistency and that there is little difference between the results of QCISD and CCSD, provided that the wave function is dominated by a single reference configuration.[53] Janowski and Pulay have recently confirmed this in the case of a qualitatively similar system (the benzene dimer), for which the intermolecular binding energies calculated at the QCISD(T) level are almost identical with results obtained by means of CCSD(T).[39]

In the following two subsections, we provide a short introduction to the interaction energy decomposition approach used and describe the various interaction models to which it was applied.

2.1. Hybrid Variation—Perturbation Interaction Energy Analysis. Theoretical details for this type of analysis and its applications published to date can be found in previous articles and in the references cited therein.[22,50,54] Essentially, a selection of interaction terms is obtained that is analogous to the ones found in state-of-the-art symmetry-adapted perturbation theory (SAPT).[55] Combined with an integral direct version of the SCF algorithm[56] and new implementation of parallelization within GAMESS (US),[57] this hybrid solution allows much larger problems to be tackled than was previously possible.

In its simplest form, a second-order Møller—Plesset (MP2) interaction energy calculation for an interacting dimer is broken down in the following way:

$$\Delta E_{MP2} = \Delta E_{el}^{(1)} + \Delta E_{ex}^{(1)} + \Delta E_{del}^{(R)} + \Delta E_{corr} \quad (1)$$

where these four components are usually interpreted as corresponding to certain quantum mechanical effects in the electronic wave function of the dimer, relative to the wave functions of isolated monomers in the dimer-centered basis set. These contributions are as follows:

$\Delta E_{el}^{(1)}$: first-order electrostatic interaction between monomer Hartree—Fock densities, unperturbed by their mutual influence

$\Delta E_{ex}^{(1)}$: the associated exchange repulsion attributed to the Pauli exclusion principle

$\Delta E_{del}^{(R)}$: charge delocalization, which includes the induction and exchange-induction effects that complement the Hartree—Fock interaction energy

ΔE_{corr}: dynamic electron correlation at the MP2 level (in this case), which includes uncoupled dispersion effects and intramolecular corrections

Summing the four terms in eq 1 successively from left to right, one obtains a series of interaction energies at different levels, rising in theoretical accuracy as well as computational cost:

$$\Delta E_{el}^{(1)} < E_{HL}^{(1)} < E_{RHF} < E_{MP2} \quad (2)$$

where $\Delta E_{HL}^{(1)} = \Delta E_{el}^{(1)} + \Delta E_{ex}^{(1)}$ is usually called the Heitler—London energy and ΔE_{RHF} is the interaction at the (restricted) Hartree—Fock level.

This analysis can be readily generalized to many-body systems, which leads to a partitioning of the various interaction energy terms into two-, three-, ..., n-body contributions, aside from the electrostatic term $\Delta E_{el}^{(1)}$ which is pairwise additive (see Góra et al.[54] for a detailed discussion and application of many-body calculations). Since many-body effects inherently include interactions between all subsets (or fragments) of a system, in the present case, they include interactions between nucleobases as well as dimers containing the intercalator. To avoid confusion, we will use $\Delta\varepsilon$ when referring to the sum of all possible many-body interaction contributions and reserve ΔE for interactions involving only the intercalator.

Since several of the cases investigated in this study involve charged species, interaction energies estimated in the gas phase will be quite different from those in a polar solvent such as water. We attempt to estimate the magnitude of such a solvent effect using the polarizable continuum model (PCM),[58] which should adequately render the electrostatic shielding of the charged phosphate groups by a polarizable environment.

To this end, the hybrid variation—perturbation scheme outlined above can be generalized to complexes in an external potential and can readily be used to study intermolecular interactions in a PCM-type solvent. The particulars of the methodology can be found in a recent article by Góra et al.[59] and references cited therein. In short, the solute molecules are placed in a cavity inside an isotropic dielectric medium, represented by apparent charges on a solvent-accessible surface. These charges give rise to an external potential that modifies the one-electron Hamiltonians of the interacting species and their complex. Consequently, their wave functions and the resulting intermolecular interactions also change, and the final value is estimated in a self-consistent procedure. In passing to the solvent, however, the basic energetic quantity is changed[58] and an additional component $\Delta\Delta G(AB)$ arises. This additional term represents indirect solvent-mediated interactions, or the

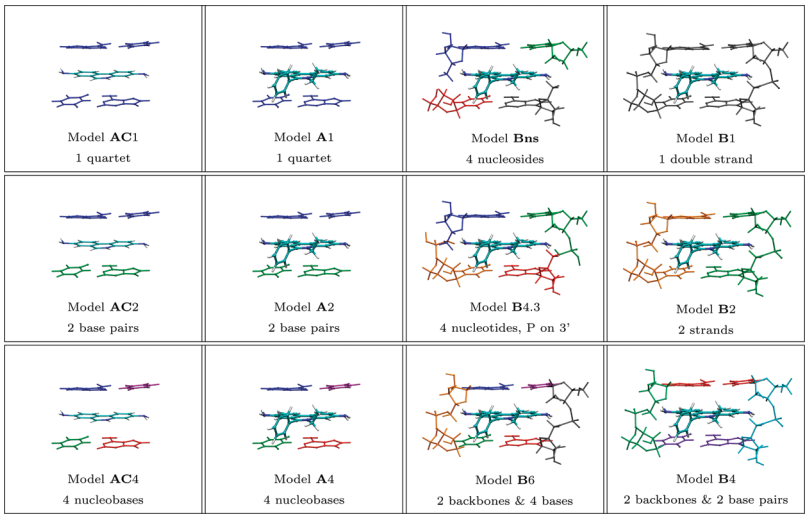

Figure 1. Schematic drawings of the models considered for the $Eth^{(+1)}$—UA/AU intercalation complex. Each color represents a piece of separately interacting RNA fragment around the binding site. The total interaction was constructed as the sum of all pairwise interactions among these pieces with the ethidium cation (see text for details).

differential free energy of solvation:

$$\Delta\Delta G(\mathrm{AB}) = \Delta G_{\mathrm{sol}}(\mathrm{AB}) - \Delta G_{\mathrm{sol}}(\mathrm{A}) - \Delta G_{\mathrm{sol}}(\mathrm{B}) \qquad (3)$$

where the terms on the right-hand side are the free energies of solvation of the complex and its constituents.

The last two quantities in eq 3 can be evaluated either in the cavity formed by a dimer or in their respective monomeric cavities. Using a dimeric cavity to evaluate $\Delta G_{\mathrm{sol}}(\mathrm{A})$ and $\Delta G_{\mathrm{sol}}(\mathrm{B})$ is in the spirit of the definition of the interaction energy,[59] and the corresponding differential free energy of solvation will therefore be referred to as $\Delta\Delta G^{\mathrm{int}}$; the value obtained using monomeric cavities will be called $\Delta\Delta G^{\mathrm{stab}}$ since conceptually it involves reorganization of the solvent due to dissociation. We also reserve the term *internal energy* for the expectation value of the gas-phase Hamiltonian using the solvent-modified wave function, following the usual PCM definition. All of the PCM results reported were estimated using the integral equation formalism version of the PCM approach (IEF-PCM), as implemented in GAMESS (US), including only electrostatic terms and assuming the standard parameters of a water solvent.

2.2. Interaction Models Used. All of the selected models are subsets of the intercalation site, which is based on an X-ray crystallographic geometry published by Jain and Sobell.[49] The crystallographic coordinates were treated here in the same way as in the previous study of this ethidium—RNA system by Langner et al.[22] In short, hydrogen atoms were added with the Reduce code,[60] and their positions were optimized in GAMESS (US)[57] using a PM3 model Hamiltonian (non-hydrogen atoms were kept frozen). Presently, we reoptimized the positions of the hydrogen atoms using the UFF force field[61] as well as DFT/B3LYP calculations. In both cases, one or several external hydrogen atoms on the RNA backbone changed their orientations, whereas no hydrogen atoms with close contacts moved more than 0.1 Å. This did not influence the interaction energies we are interested in by more than 0.2 kcal/mol (data not shown), and we thus retained the PM3 coordinates of hydrogen atoms for consistency.

The system was divided into fragments in several ways, most of which are illustrated by the schematic representations in Figure 1. Names beginning with **A** were limited to the ethidium molecule and four neighboring base pairs. Model **AC**4 is the smaller, previously used version,[22] which contains only the ethidium chromophore. The **A**4 variant labeled additionally *parts* considers the entire ethidium molecule but divides it into three parts—its chromophore, side chain, and ring. The versions with **B** in their names include the sugars and phosphate groups connecting the base pairs, whereas the intermediate model **Bns** disregards the phosphate groups and represents the RNA fragment only by nucleosides (adenosine or uridine).

There is an additional number (N_{int}) in each name (e.g., 1 or 4 in **AC**1 or **AC**4) that denotes the actual number of RNA—intercalator dimers evaluated when estimating the interaction energy ΔE in a pairwise fashion. In Figure 1, the subsystems in each case are indicated by different colors. For clarity, we also append this number to the name of the largest models, so that **A**1 stands for the case where the interaction energy of ethidium was evaluated with all four nucleobases in a single calculation (one dimer).

Whenever the number of interacting dimers N_{int} was more than one, the interactions of the intercalator with each RNA fragment were summed in a pairwise fashion. For instance, in the case of **A**2, the total pair interaction energy consists of two parts, corresponding to uncoupled contributions from the interaction of ethidium with two base pairs:

$$\Delta E_{\mathrm{A2}} = \Delta E_{\mathrm{Eth}\ldots\mathrm{A/U}} + \Delta E_{\mathrm{Eth}\ldots\mathrm{U/A}} \qquad (4)$$

where ΔE can be substituted by the interaction energy at any chosen level of theory, or by any term from eq 2.

The interaction energies on the right-hand side of eq 4 are estimated in different dimer-centered basis sets, and this rule was adopted for all of the models used. Therefore, the pairwise interaction energies of **A**2 and **A**4 differ from that of model **A**1 not only due to neglect of many-body interactions but also by virtue of basis set extension effects. The same is true when comparing **B**1 to **B**2 or **B**4 or to any of the other variants.

In contrast to the **A**-type models, differences can also arise due to capping effects when phosphate groups are included. For

example, in the **B**4- and **B**6-type models, four covalent bonds are severed, between each nucleobase and the sugar residue it is attached to, and the cut bonds are hydrogenated with protons. This means that in these two cases the intercalator effectively interacts with four extra nuclei and electrons compared to **B**1. In **B**4.3 and **B**4.5 on the other hand, two bonds were cut, between the phosphate groups and sugar residues at the 3′ (closer to uracil) and 5′ (closer to adenine) ends, respectively. Therefore, in **B**4.3, both phosphate groups were in the same monomer as adenosines, while in model **B**4.5, they were attached to uridines. In all of these cases where bonds were cut, the positions of the capping hydrogen atoms were optimized using the UFF force field.

Furthermore, the phosphate groups in the **B** class of interaction models were considered in several variants with respect to their charge state, specified by additional labels and illustrated in Figure 2. In models labeled as *neutral (H)*, the anionic phosphate groups were neutralized by attaching protons to the most anionic oxygen, as has been practiced in the literature.[21] Variants quenched with counterions were also prepared, in which the positions of Na^+ and K^+ were optimized near each phosphate group—these are labeled *neutral (Na)* and *neutral (K)*. In the interaction models labeled *charged −2*, the charge on the RNA fragment was left entirely unbalanced, and *charged −2 (H_2O)* indicates that both anionic groups were hydrated with single water molecules (one per phosphate group). The position of the additional proton in the *neutral (H)* variant was optimized using the UFF force field, and counterions and water molecule positions were optimized at the DFT/B3LYP level in the vicinity of the relevant RNA backbone fragment, which was kept fixed.

3. RESULTS AND DISCUSSION

3.1. Pair-Wise Models. In all of the models tested (**AC**, **A**, **Bns**, **B**, and their variants), dividing the RNA fragment into nucleobases and backbone strands or into nucleotides is justified from the energetic point of view (Table 1). For the neutral models, partitioning of the system in this way changes the total interaction by no more than 2%. In particular, for the smallest **AC**-type models, the difference between the sum of pairwise interactions (the ethidium chromophore with each nucleobase separately, **AC**4) and the interaction calculated with all four nucleobases at once (**AC**1) was 0.4 kcal/mol. For the model including the ethidium side chain and ring (**A**), the analogous difference between **A**4 and **A**1 was only 0.2 kcal/mol. Such small differences indicate that, while the properties of adenine−uracil base pairs may be significantly changed from that of single nucleobases, this does not noticeably influence their interactions with ethidium.

The largest error associated with a pairwise approximation of the interaction energy was found in the case of the charged version (**B**·charged −2), around 8 kcal/mol or 6% for **B**4.5 compared to **B**1. This relatively large difference is understandable, since the delocalization of unbalanced charge is hindered more strongly when fragmentation occurs near the phosphate groups. Separating the two strands (as in **B**2) already increases the interaction by almost 5 kcal/mol.

All these conclusions hold for both the total interaction energy at the MP2 level as well as the particular components into which it is divided, although the electrostatic part $\Delta E_{el}^{(1)}$ seems to be the most affected by fragmentation. The good performance of such a pairwise approximation provoked us to calculate the nonadditive

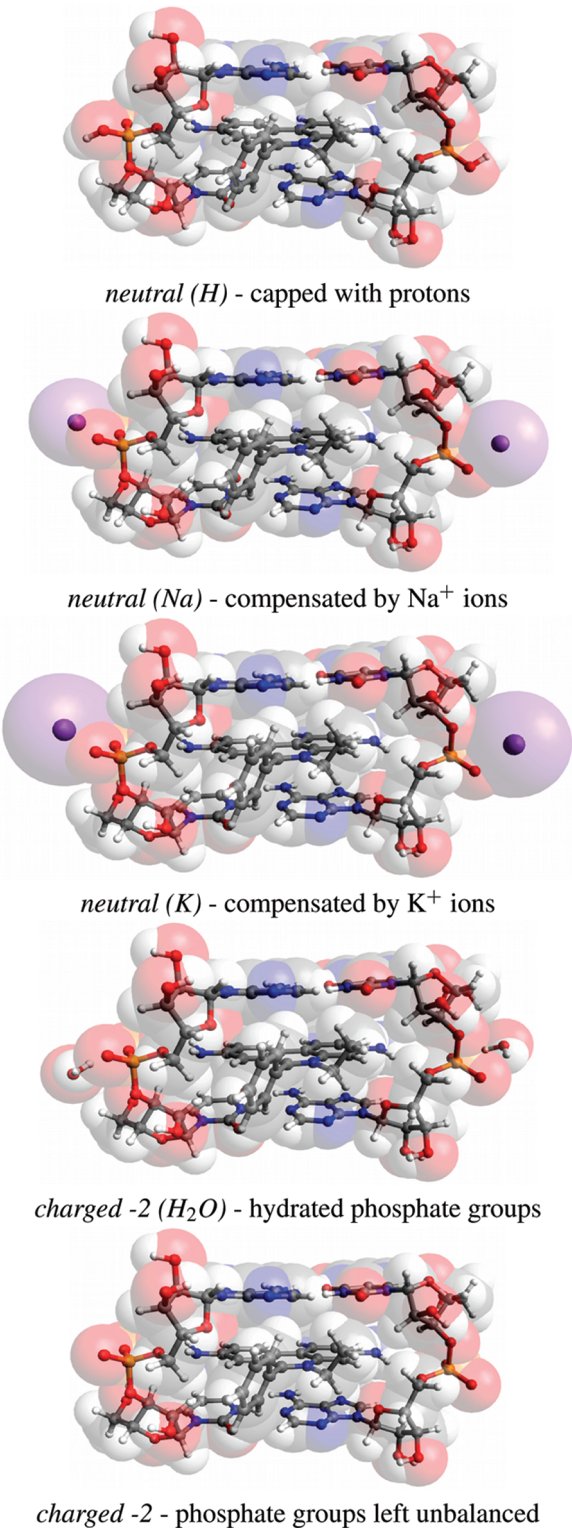

Figure 2. The five phosphate group variants considered in this work, in the order of increasing interaction energy (from top to bottom) for the intercalated ethidium cation in the gas phase (according to Table 1).

contributions to the interaction energy at the Hartree−Fock level and its components for the models **AC** and **A** (containing ethidium or its chromophore and four nucleobases) as well as for selected **B** variants (ethidium with two dinucleotides). Since in

Table 1. Components of the Interaction Energy for the Eth$^{(+1)}$−UA/AU Intercalation Complex in the Gas Phase Following eq 1 in the Text[a]

	N_{int}	N_{AO}	$\Delta E_{el}^{(1)}$	$\Delta E_{ex}^{(1)}$	$\Delta E_{del}^{(R)}$	ΔE_{corr}	ΔE_{MP2}
model **AC**1	1	878	−24.8	31.8	−4.8	−33.4	−31.3
model **AC**2	2	615	−25.3	32.0	−4.7	−33.5	−31.5
model **AC**4	4	475	−26.0	32.3	−4.7	−33.3	−31.7
model **A**1	1	1030	−28.6	40.2	−6.1	−39.7	−34.3
model **A**2	2	733	−28.9	40.2	−6.0	−39.4	−34.2
model **A**4	4	601	−29.8	40.7	−6.2	−39.2	−34.5
model **A**4 (parts)	12	475	−30.1	41.6	−6.4	−39.6	−34.5
model **Bns**	4	753	−35.7	51.7	−10.6	−51.9	−46.6
model **B**1·neutral (H)	1	1776	−41.9	54.9	−10.9	−54.7	−52.6
model **B**2·neutral (H)	2	1106	−43.0	55.4	−11.1	−54.4	−53.1
model **B**4·neutral (H)	4	829	−42.6	55.7	−11.1	−54.7	−52.7
model **B**6·neutral (H)	6	829	−43.5	56.2	−11.3	−54.4	−52.9
model **B**4.3·neutral (H)	4	799	−43.5	56.7	−12.1	−54.7	−53.6
model **B**4.5·neutral (H)	4	832	−40.3	46.2	−10.5	−49.4	−54.0
model **B**1·neutral (Na)	1	1802	−50.7	55.1	−10.9	−55.0	−61.5
model **B**1·neutral (K)	1	1830	−52.7	55.1	−10.9	−55.1	−63.6
model **B**1·charged −2 (H_2O)	1	1814	−117.1	55.2	−11.0	−56.4	−129.3
model **B**1·charged −2	1	1766	−121.1	55.2	−11.1	−56.5	−133.5
model **B**2·charged −2	2	1101	−123.5	56.0	−13.9	−56.6	−138.0
model **B**4·charged −2	4	824	−122.5	56.5	−15.8	−57.1	−138.9
model **B**6·charged −2	6	824	−123.3	57.0	−16.0	−56.8	−139.2
model **B**4.3·charged −2	4	794	−126.0	56.7	−15.2	−57.0	−141.6
model **B**4.5·charged −2	4	827	−120.5	46.5	−15.5	−51.8	−141.2

[a] The symbols in the left column correspond to various molecular interaction models as illustrated in Figure 1 and described in the text. The column N_{int} contains the number of pair-wise calculations comprising the interaction, and N_{AO} denotes the maximum number of atomic orbitals used in any pair-wise calculation within a particular model. All energies were obtained using the 6-31G** basis set, and are given in kcal/mol.

these cases there is no capping or overlap between fragments, the interaction energy can be expressed as a sum of pairwise and nonadditive components evaluated consistently in the basis set of the entire system. The results of these calculations (Table 2) show that all of the nonadditive terms are virtually negligible and that the observed consistency of the full and fragmented models in Table 1 is in fact due to the small magnitude of these effects and not to a fortuitous cancellation of errors. The nonadditivities are also small in the case of **B**-type models, in which the charged phosphate groups are either compensated by counterions or hydrated. Only in the latter case, the nonadditive polarization effects are larger, since hydration does not quench the excess charge as effectively as compensation by protons or counterions. And in this case, the pairwise approximation overestimates the extent of delocalization effects by approximately 12%, while for the other studied systems, this error is between 2% and 5%.

It needs to be stressed that the nonadditivities discussed above include interactions between all nucleobases (or strands) alongside ethidium−nucleobase (or strand) interactions and thus are not directly comparable to the primary results of this work, which include only the latter. To illustrate this point explicitly, consider ΔE_{RHF} in the **AC**-type models, that is, the energy obtained by bringing the intercalator from infinity into its position between the base pairs, assuming there are no relaxation or deformation effects. On the other hand, $\Delta\varepsilon_{RHF}$ is the energy needed to simultaneously dissociate all five molecules of the intercalation site. Nonetheless, the nonadditivities that exist in $\Delta\varepsilon_{RHF}$ ($\Delta^3\varepsilon_{ex}^{(1)}$, $\Delta^3\varepsilon_{del}^{(R)}$, and higher order terms) are inherent also to ΔE_{RHF}, so it is worthwhile to show that they are small. Our goal here, however, is not to provide precise values but rather to confirm that these effects are in fact small, since this in turn confirms that the effects of nucleobase polarization are similarly small.

Table 2. Many-Body Partitioning of the Total Interaction Energy for the Eth$^{(+1)}$-UA/AU Intercalation Complex[a]

	$\Delta\varepsilon_{el}^{(1)}$	$\Delta^2\varepsilon_{ex}^{(1)}$	$\Delta^3\varepsilon_{ex}^{(1)}$	$\Delta^2\varepsilon_{del}^{(R)}$	$\Delta^3\varepsilon_{del}^{(R)}$	$\Delta\varepsilon_{RHF}$
model **AC**	−90.6	108.0	0.0	−32.4	0.8	−14.2
model AC/aug-cc-pVDZ	−87.5	109.1	0.0	−35.2	1.3	−12.5
model **A**	−94.5	116.6	−0.2	−33.9	1.1	−10.9
model **B**·neutral (Na)	−117.1	132.1	−0.2	−38.9	1.7	−22.4
model **B**·neutral (K)	−119.0	132.2	−0.2	−39.0	1.8	−24.2
model **B**·charged −2 (H_2O)	−161.8	134.1	−0.2	−42.0	4.8	−65.1

[a] Δ^n, where n = 2, 3, 4+, denotes two-, three- and higher-order many-body effects, respectively. In contrast to ΔE_{RHF} and other values given in Table 1, these interaction energies include not only ethidium−nucleobase (or ethidium−strand) interactions but also nucleobase−nucleobase or strand−strand interactions; hence, the two are not directly comparable. In the **B**-type models, counterions (or water molecules) together with the corresponding strands were treated as single monomers. In all cases, energies are in kcal/mol, and four-body and higher contributions, namely, $\Delta^{(4+)}\varepsilon_{ex}^{(1)}$ and $\Delta^{(4+)}\varepsilon_{del}^{(R)}$, were insignificantly small and are therefore omitted here. Unless otherwise noted, all results were obtained using the 6-31G** basis set.

It is known that in order to accurately evaluate many-body effects beyond the Hartree−Fock level correlated methods higher than MP2 need to be employed. This point has been recently demonstrated for a uracil tetramer,[62] although the magnitude of these effects remains a fraction of the total interaction energy. This may be attributed to an intrinsically local nature of electron correlation effects, and therefore we expect similar magnitudes for the systems studied here. Furthermore, Ghosh et al.[44] have demonstrated that for oligomers of nucleic acid bases pairwise interactions between only nearest neighbors are a sufficient approximation. Combined with our results, this opens a potential efficient route for calculations of intercalators bound to entire nucleic acid strands.

Recently, Hill and Platts reported similar considerations for three intercalators, ethidium being among them.[28] They compared interaction energies calculated for the intercalator between two base pairs separately and for the entire base pair step, which respectively correspond to **A**2 and **A**1 in our case. Interestingly, they also found only small differences between the two for ethidium, although in their case, the molecule was intercalated in the AT/AT step and slightly different methods and basis sets were used. They reported larger deviations in the case of daunomycin situated between GC/GC base pairs, namely, around +5 kcal/mol or 15% of the interaction energy with both base pairs. Therefore, the question remains whether these deviations originate from different properties of GC base pairs compared to AT or AU, or rather from differences between the chromophores of these intercalators. In any case, the accuracy of this type of fragmentation will depend heavily on the molecular details and cannot be recommended for all scenarios.

3.2. Electron Correlation Corrections. It is well established that the MP2 method overestimates the dispersion part of stacking interaction energies, due to missing response effects,[27] and it is now quite common to correct for this. [In general, perturbative corrections are doomed to fail for conductors where the HOMO−LUMO gap goes to zero and energy denominators accordingly diverge. This effect is partially responsible for the deteriorating quality of MP2 results as the sizes of aromatic systems increase and orbitals become more delocalized.] Here, we perform additional QCISD(T) calculations for the smallest, nonfragmented (**AC**1) and fragmented (**AC**4) models in order to assess the extent of these effects (Table 3). A correction of around 9 kcal/mol is obtained (about 30% of both ΔE_{corr} and ΔE_{MP2} for models **AC** and **A**). Surprisingly, the contribution of triple excitations is relatively minor compared to polycyclic aromatic hydrocarbons such as the recently studied coronene dimer,[43] although this difference might be caused by the limited basis set used here. Another reason might be the fact that that the system under study consists of separate molecules, smaller than coronene. In any case, the description provided by MP2 is quite accurate here, closer in quality to the benzene dimer and other small aromatic systems. Although the largest model studied here (**AC**1) is not small, the $\pi-\pi$ stacking interaction of the ethidium cation decomposes easily into smaller, pairwise components between the intercalator and separate nucleobases.

On the other hand, dispersion interactions are also quite difficult to saturate with respect to the basis set,[30,38] and in our case, an additional −17 kcal/mol are added to the MP2 interaction energy for model **AC**1 when 6-31G** is replaced with aug-cc-pVDZ (Table 3). Combined with the 9 kcal/mol correction discussed above (connected to the overestimation of dispersion by MP2 that is relatively unaffected by basis set extension), this gives an overall correction of about −8 kcal/mol. Since these effects are essentially local in nature, we shall assume that this correction is also applicable to **B**-type models. This gives a corrected gas phase interaction energy of roughly −61 kcal/mol for model **B**·neutral (H) and −142 kcal/mol for **B**·charged −2. For comparison, Kubař et al.[21] also reported a correlated (RI-MP2) interaction energy of −70 kcal/mol for ethidium between an AT/TA step in a system corresponding to the present **B**·neutral (H). We also tested the modified basis set 6-31G** (d = 0.25), where d functions were made more diffuse by lowering their exponents from 0.8 to 0.25, as well as the smaller basis set 6-31G* (d = 0.25) that is more widespread (see the Supporting Information), and both of these produced correlation energies close to the aug-cc-pVDZ basis set. Although electron correlation effects are dominant and in fact are the origin of stabilization in the case of the smaller neutral models, where ΔE_{RHF} is repulsive, it is the electrostatic component that differentiates between different charge states of the phosphate groups in the gas phase. An analogous observation has been made for 16 stacked DNA bases,[63] where relative stabilities correlate more strongly with the electrostatic term than with the dominant dispersion component.

Table 3. Interaction Energy at Various Levels of Theory for Models AC1 and AC4 of the Eth$^{(+1)}$−UA/AU Intercalation Complex in the Gas Phase (All Values in kcal/mol)[a]

model/basis set	$\Delta E_{el}^{(1)}$	$\Delta E_{HL}^{(1)}$	ΔE_{RHF}	ΔE_{MP2}	ΔE_{QCISD}	$\Delta E_{QCISD(T)}$
AC1/6-31G**	−24.8	7.0	2.1	−31.3	−18.1	−22.0
AC4/6-31G**	−26.0	6.3	1.7	−31.3	−18.4	−22.4
AC1/6-31G** (d = 0.25)	−24.5	6.4	0.8	−44.3	−28.3	−33.9
AC4/6-31G** (d = 0.25)	−25.5	5.7	0.0	−44.7	−29.1	−34.7
AC4/aug-cc-pVDZ	−25.1	7.6	1.0	−48.8	−32.2	−39.2

[a] The triples contribution, and consequently QCISD(T), for **AC**1/aug-cc-pVDZ is expected to be within 1 kcal/mol of **AC**4/aug-cc-pVDZ and was judged too expensive to calculate (see the Supporting Information for details).

3.3. Phosphate Group Charge and Solvation Effects. As already mentioned, several variants of the extended model **B** were considered. In the first case, *neutral (H)*, the anionic phosphate groups were neutralized by protonation. Quenching by adding one of two counterions (Na^+ or K^+) to each phosphate group was designated as *neutral (Na)* and *neutral (K)*. The *charged −2* model on the other hand leaves the phosphate groups charged or hydrated by a single water molecule. In order to consider the relevance of these different situations, one should keep in mind the significant fluctuations an intercalation site and its surroundings may undergo in solution, and that it has been shown that the movement of counterions is diffusive around DNA.[32,33] Therefore, the quenching in models **B** (Na^+) and **B** (K^+) is at best a temporary configuration. At times when no counterion is present in the immediate vicinity of a phosphate group, it will simply be hydrated.

Our results show that monohydration damps the interaction compared to bare charged phosphate groups only slightly (about +5 kcal/mol). Hydration with further water molecules should increase this effect, and counterions that are farther away may still quench them indirectly by polarizing adjacent water molecules. In an attempt to estimate the effect of solvation, we performed PCM calculations at the Hartree−Fock level in selected cases

Table 4. The Effect of Polarizable Continuum Model (IEF-PCM) Solvation on the Interaction Energy at Various Levels of Theory for Neutral and Charged Variants of Model B1[a]

		$\Delta E_{el}^{(1)}$	$\Delta E_{ex}^{(1)}$	$\Delta E_{del}^{(R)}$	$\Delta\Delta G_{RHF}^{int}$	ΔE_{corr}	ΔE_{MP2}
model **B1**·neutral (Na)	in vacuum	−50.7	55.1	−10.9		−55.0	−61.5
	in solvent	−58.2	56.6	−6.7	29.0 (21.2)		*−34.3(−42.1)*
model **B1**·neutral (K)	in vacuum	−52.7	55.1	−10.9		−55.1	−63.6
	in solvent	−60.5	56.6	−6.7	31.2 (23.5)		*−34.5(−42.2)*
model **B1**·charged −2 (H_2O)	in vacuum	−117.1	55.2	−11.0		−56.4	−129.3
	in solvent	−122.3	56.6	−7.2	92.7 (84.8)		*−36.6(−44.5)*

[a] The $\Delta\Delta G_{RHF}^{int}$ values in parentheses are the corresponding $\Delta\Delta G_{RHF}^{stab}$ energies; ΔG_{MP2} values in italics were estimated assuming the gas phase ΔE_{corr} energies. All energies were obtained using the 6-31G** basis set, and are given in kcal/mol. See the text for further details.

(Table 4). The individual components of the internal interaction energy are not substantially modified when passing to the solvent. In particular, one notes a slight increase in $\Delta E_{el}^{(1)}$, which is balanced by an increase in exchange-repulsion and a decrease in $\Delta E_{del}^{(R)}$. The resulting internal interaction energy has almost the same magnitude as its gas phase counterpart.

The polarizable environment, however, shields the electrostatic interactions to a large extent, and in effect the Hartree−Fock interaction free energies ΔG_{RHF} are repulsive, close to 20 kcal/mol for all three chosen models. It should be noted that more than 90% of the $\Delta\Delta G_{RHF}^{int}$ coupling term comes from the corresponding Heitler−London component which includes electrostatic interactions with the polarized solvent. Therefore, $\Delta\Delta G_{RHF}^{int}$ can be interpreted as an effective correction to the $\Delta E_{el}^{(1)}$ term. Although we did not compute the corresponding solvent-adjusted ΔE_{corr} terms, these should not differ much from their gas phase counterparts. We therefore roughly estimate the interaction free energy ΔG_{MP2} for all of the cases presented in Table 4 to be −35 kcal/mol and the alternate $\Delta\Delta G^{stab}$ calculated using monomeric cavities in eq 3 to be about −43 kcal/mol. It should be stressed that the approximations made here are quite crude, and we do not aim to establish quantitative results. This is impossible, since the PCM method was not parametrized for such systems and the result will depend heavily on the choice of the solute cavities. We also neglect the effects of geometry relaxation here and account only for the electrostatic contribution to the free energy required to bring the interacting molecules from an infinite separation to the complex in a dilute solvent.

Nonetheless, a particularly intriguing observation is that the polarizable environment seems to equate all of the considered charge states of the phosphate groups. What relevance then does the large magnitude of the gas phase interaction energy in the case of the charged models have? This is an especially pertinent question since the overall binding free energies for various intercalators are typically estimated around −10 kcal/mol by both experimental[9] and theoretical[16] methods. Moreover, the final phase of intercalation—insertion of the planar chromophore between two base pairs—facilitates significant changes in the hydration shell and entails a significant free energy barrier.[8] If the charge density around the phosphate groups fluctuates as a result, the instantaneous interactions may intensify in a way reminiscent of the charged models studied here. Therefore, our results can be viewed as identifying the broadest range of intermolecular interaction strengths possible for this conformation of the intercalation site with **B**·*neutral (H)* and **B**·*charged* −2 giving the approximate lower and upper limits. It would be interesting to confront the present static scenario with a dynamic range that takes conformational changes of the binding site and surrounding solvent molecules into account on equal footing.

4. CONCLUSIONS

In this contribution we have taken a detailed look at the intermolecular interactions in the intercalation site $Eth^{(+1)}$−UA/AU, which consists of the ethidium cation and the RNA AU/UA base pair step, built on the basis of crystallographic data. We consider the effect of dividing the system into fragments and calculating *ab initio* interaction energies in a pairwise fashion, as well as many-body effects and the influence of phosphate group quenching by various surroundings. We also explore the effects of solvation on these interactions by assuming a polarizable continuum model of water around the intercalation site.

Our results can be summarized in three basic conclusions, the first pertaining to system fragmentation into parts interacting pairwise with the intercalator. Namely, the various ways chosen of partitioning the system reproduce the supermolecular interaction energy within a few percent, even when the anionic phosphate groups are left unbalanced. But not all of the interaction models are equal in this regard. For example, breaking the RNA strand into backbone and/or nucleobase fragments (as in **B2** and **B6**) results in interaction energies closer to model **B1** than when the strands are split near the phosphate groups (as for example in **B4.3** and **B4.5**). It is important to remember that the success of such fragmentation schemes varies on a case-by-case basis, so we cannot recommend it as a general approach. Specifically, the present exploration of interaction models allows us to conclude that the previously adopted partitioning scheme[22] was satisfactory, as far as the energetics of the intercalator itself are concerned.

A second outcome, concerning the electron correlation part of the $\pi-\pi$ stacking interaction with the nucleobases, is the addition of almost −10 kcal/mol to the correlated interaction energy in model **AC**. This result was obtained by additional calculations at the QCISD(T) level of theory and employing more saturated basis sets.

Finally, for differently quenched phosphate groups, we estimate the possible range of interactions experienced by ethidium in the gas phase for this particular intercalation site conformation, roughly 60−140 kcal/mol. On the one hand, capping the phosphate group with a hydrogen atom mimics an overly tightly bound counterion and represents the weakest possible interaction of the cationic intercalator with the RNA backbone. Conversely, leaving the charge on the phosphate groups unbalanced represents the strongest possible interaction. Quenching with counterions and hydrating with water molecules leads to

intermediate interaction energies, and in fact we find that all of these cases produce interaction energies between the two extremes. Including solvation via a PCM method has the intuitive effect of shielding electrostatic interactions and bringing the interaction energies in these different models to comparable values, namely, around −35 kcal/mol. The disparity between this and the wide range found in the gas phase suggests that the forces acting on the intercalator during insertion may depend heavily on conformational changes and fluctuations in the hydration shell.

It is important to keep in mind that these results were obtained for a single crystallographic binding site conformation and could likely be changed by dynamic effects. In this study, we focused on the intermolecular *interaction energy* ΔG_{mol}, calculated for structures that are fully prepared for the insertion of the intercalator. Intercalation inevitably involves the untwisting of the helix and other deformations that present a significant endothermic contribution to the total free energy, as well as hydration and potentially other effects. Therefore, the impact of our results, and ΔG_{mol} in general, on intercalation energetics should be considered in the context of these other contributions that make up the total binding free energy.

■ ASSOCIATED CONTENT

Supporting Information. More detailed interaction energy decomposition results (all components of pairwise interaction models), as well as the Cartesian coordinates of the intercalation site used in our calculations. This material is available free of charge via the Internet at http://pubs.acs.org.

■ AUTHOR INFORMATION

Corresponding Author
*E-mail: Andrzej.Sokalski@pwr.wroc.pl.

■ ACKNOWLEDGMENT

K.M.L. and R.W.G. are indebted to the staff at Wrocław Center for Networking and Supercomputing for a generous allotment of computing resources and technical assistance and Wrocław University of Technology for support. This work was also supported by the National Science Foundation under award number CHE-0911541 and by the Mildred B. Cooper Chair at the University of Arkansas. Acquisition of the Star of Arkansas supercomputer was supported in part by the National Science Foundation under award number MRI-0722625.

■ REFERENCES

(1) Lerman, L. S. *J. Mol. Biol.* **1961**, *3*, 18–30.
(2) Waring, M. J. *J. Mol. Biol.* **1965**, *13*, 269–282.
(3) Strekowski, L.; Wilson, B. *Mutat. Res.* **2007**, *623*, 3–13.
(4) (a) Brano, M. F.; Cacho, M.; Gradillas, A.; de Pascual-Teresa, B.; Ramos, A. *Curr. Pharm. Des.* **2001**, *7*, 1745–1780. (b) Ferguson, L. R.; Denny, W. A. *Mutat. Res.* **2007**, *623*, 14–23. (c) Neto, B. A. D.; Lapis, A. A. M. *Molecules* **2009**, *14*, 1725–1746.
(5) (a) Guttman, A.; Cooke, N. *Anal. Chem.* **1991**, *63*, 2038–2042. (b) Chen, W.; Turro, N. J.; Tomalia, D. A. *Langmuir* **2000**, *16*, 15–19.
(6) (a) Starčevic, K.; Karminski-Zamola, G.; Piantanida, I.; Žinić, M.; Šuman, L.; Kralji, M. *J. Am. Chem. Soc.* **2005**, *127*, 1074–1075. (b) Stojkovič, M. R.; Marczi, S.; Glavaš-Obrovac, L.; Piantanida, I. *Eur. J. Med. Chem.* **2010**, *45*, 3281–3292.
(7) Horowitz, E. D.; Engelhart, A. E.; Chen, M. C.; Quarles, K. A.; Smith, M. W.; Lynn, D. G.; Hud, N. V. *Proc. Natl. Acad. Sci.* **2010**, *107*, 5288–5293.
(8) Mukherjee, A.; Lavery, R.; Bagchi, B.; Hynes, J. T. *J. Am. Chem. Soc.* **2008**, *130*, 9747–9755.
(9) Breslauer, K. J.; Remeta, D. P.; Chou, W.-Y.; Ferrante, R.; Curry, J.; Zaunczkowski, D.; Snyder, J. G.; Marky, L. A. *Proc. Natl. Acad. Sci.* **1987**, *84*, 8922–8926.
(10) Graves, D. E.; Velea, L. M. *Curr. Org. Chem.* **2000**, *4*, 915–929.
(11) Kostjukov, V. V.; Khomytova, N. M.; Evstigneev, M. P. *Biopolymers* **2009**, *91*, 773–790.
(12) Chaires, J. B. *Arch. Biochem. Biophys.* **2006**, *453*, 26–31.
(13) Misra, V. K.; Honig, B. *Proc. Natl. Acad. Sci.* **1995**, *92*, 4691–4695.
(14) Elcock, A. H.; Rodger, A.; Richards, W. G. *Biopolymers* **1996**, *39*, 309–326.
(15) Resat, H.; Mezei, M. *Biophys. J.* **1996**, *71*, 1179–1190.
(16) Bagiński, M.; Fogolari, F.; Briggs, J. M. *J. Mol. Biol.* **1997**, *274*, 253–267.
(17) Medhi, C.; Mitchell, J. B. O.; Price, S. L.; Tabor, A. B. *Biopolymers* **1999**, *52*, 84–93.
(18) Bondarev, D. A.; Skawinski, W. J.; Venanzi, C. A. *J. Phys. Chem. B* **2000**, *104*, 815–822.
(19) Řeha, D.; Kabeláč, M.; Ryjáček, F.; Šponer, J.; Šponer, J. E.; Elstner, M.; Suhai, S.; Hobza, P. *J. Am. Chem. Soc.* **2002**, *124*, 3366–3376.
(20) Hobza, P.; Šponer, J. E. *Chem. Rev.* **1999**, *99*, 3247–3276.
(21) Kubař, T.; Hanus, M.; Ryjáček, F.; Hobza, P. *Chem.—Eur. J.* **2006**, *12*, 280–290.
(22) Langner, K. M.; Kędzierski, P.; Sokalski, W. A.; Leszczyński, J. *J. Phys. Chem. B* **2006**, *110*, 9720–9727.
(23) Dračinský, M.; Castaño, O. *Phys. Chem. Chem. Phys.* **2004**, *6*, 1799–1805.
(24) Xiao, X.; Cushman, M. *J. Am. Chem. Soc.* **2005**, *127*, 9960–9961.
(25) (a) Tuttle, T.; Kraka, E.; Cremer, D. *J. Am. Chem. Soc.* **2005**, *127*, 9469–9484. (b) Barone, G.; Guerra, C. F.; Gambino, N.; Silvestri, A.; Lauria, A.; Almerico, A. M.; Bickelhaupt, F. M. *J. Biomol. Struct. Dyn.* **2008**, *26*, 115–129. (c) Li, S.; Cooper, V. R.; Thonhauser, T.; Lundqvist, B. I.; Langreth, D. C. *J. Phys. Chem. B* **2009**, *113*, 11166–11172.
(26) Fantacci, S.; Angelis, F. D.; Sgamellotti, A.; Marrone, A.; Re, N. *J. Am. Chem. Soc.* **2005**, *127*, 14144–14145.
(27) Cybulski, S. M.; Lytle, M. L. *J. Chem. Phys.* **2007**, *127*, 141102.
(28) Hill, J. G.; Platts, J. A. *Chem. Phys. Lett.* **2009**, *479*, 279–283.
(29) Šponer, J.; Jurečka, P.; Marchan, I.; Luque, F. J.; Orozco, M.; Hobza, P. *Chem.—Eur. J.* **2006**, *12*, 2854–2865.
(30) Pitoňák, M.; Janowski, T.; Neogrády, P.; Pulay, P.; Hobza, P. *J. Chem. Theory Comput.* **2009**, *5*, 1761–1766.
(31) Horowitz, E. D.; Lilavivat, S.; Holladay, B. W.; Germann, M. W.; Hud, N. V. *J. Am. Chem. Soc.* **2009**, *131*, 5831–5838.
(32) Varnai, P.; Zakrzewska, K. *Nucleic Acids Res.* **2004**, *32*, 4269–4280.
(33) Kirmizialtin, S.; Elber, R. *J. Phys. Chem. B* **2010**, *114*, 8207–8220.
(34) Svozil, D.; Hobza, P.; Šponer, J. *J. Phys. Chem. B* **2010**, *114*, 1191–1203.
(35) Kolar, M.; Kubař, T.; Hobza, P. *J. Phys. Chem. B* **2010**, *114*, 13446–13454.
(36) Pople, J. A.; Head-Gordon, M.; Raghavachari, K. *J. Chem. Phys.* **1987**, *87*, 5968–5975.
(37) Jurečka, P.; Šponer, J.; Černý, J.; Hobza, P. *Phys. Chem. Chem. Phys.* **2006**, *8*, 1985.
(38) Riley, K. E.; Pitoňák, M.; Jurečka, P.; Hobza, P. *Chem. Rev.* **2010**.
(39) Janowski, T.; Pulay, P. *Chem. Phys. Lett.* **2007**, *447*, 27–32.
(40) Fiethen, A.; Jansen, G.; Hesselmann, A.; Schütz, M. *J. Am. Chem. Soc.* **2008**, *130*, 1802–1803.
(41) ElSohly, A. M.; Hopkins, B. W.; Copeland, K. L.; Tschumper, G. S. *Mol. Phys.* **2009**, *108*, 923–928.
(42) Singh, N. J.; Min, S. K.; Kim, D. Y.; Kim, K. S. *J. Chem. Theory Comput.* **2009**, *5*, 515–529.
(43) Janowski, T.; Ford, A. R.; Pulay, P. *Mol. Phys.* **2010**, *108*, 249–257.

(44) Ghosh, D.; Kosenkov, G.; Vanovschi, V.; Williams, C. F.; Herbert, J. M.; Gordon, M. S.; Schmidt, M. W.; Slipchenko, L. V.; Krylov, A. I. *J. Phys. Chem. A* **2010**, *114*, 12739–12754.
(45) Pulay, P. *Chem. Phys. Lett.* **1983**, *100*, 151.
(46) Fedorov, D. G.; Kitaura, K. *J. Phys. Chem. A* **2007**, *111*, 6904–6914.
(47) Hohenstein, E. G.; Sherrill, C. D. *J. Chem. Phys.* **2010**, *132*, 184111.
(48) Platts, J. A.; Hill, J. G. *Mol. Phys.* **2010**, *108*, 1497–1504.
(49) Jain, S. C.; Sobell, H. M. *J. Biomol. Struct. Dyn.* **1984**, *1*, 1161–1177.
(50) Sokalski, W. A.; Roszak, S.; Pecul, K. *Chem. Phys. Lett.* **1988**, *153*, 153–159.
(51) Boys, S. F.; Bernardi, F. *Mol. Phys.* **2002**, *100*, 65–73.
(52) (a) Janowski, T.; Ford, A. R.; Pulay, P. *J. Chem. Theory Comput.* **2007**, *3*, 1368–1377. (b) Janowski, T.; Pulay, P. *J. Chem. Theory Comput.* **2008**, *4*, 1585–1592.
(53) Lee, T. J.; Rendell, A. P.; Taylor, P. R. *J. Phys. Chem.* **1990**, *94*, 5463–5468.
(54) Góra, R. W.; Sokalski, W. A.; Leszczyński, J.; Pett, V. B. *J. Phys. Chem. B* **2005**, *109*, 2027–2033.
(55) Jeziorski, B.; Moszyński, R.; Szalewicz, K. *Chem. Rev.* **1994**, *94*, 1887–1930.
(56) (a) Almlöf, J.; Faegri, K.; Korsell, K. *J. Comput. Chem.* **1982**, *3*, 385–599. (b) Haser, M.; Ahlrichs, R. *J. Comput. Chem.* **1989**, *10*, 104–111.
(57) Schmidt, M. W.; Baldridge, K. K.; Boatz, J. A.; Elbert, S. T.; Gordon, M. S.; Jensen, J. H.; Koseki, S.; Matsunaga, N.; Nguyen, K. A.; Su, S. J.; Windus, T. L.; Dupuis, M.; Montgomery, J. A. *J. Comput. Chem.* **1993**, *14*, 1347–1363.
(58) Tomasi, J.; Mennucci, B.; Cammi, R. *Chem. Rev.* **2005**, *105*, 2999–3093.
(59) Góra, R. W.; Bartkowiak, W.; Roszak, S.; Leszczynski, J. *J. Chem. Phys.* **2004**, *120*, 2802–2813.
(60) Word, J. M.; Lovell, S. C.; Richardson, J. S.; Richardson, D. C. *J. Mol. Biol.* **1999**, *285*, 1735–1747.
(61) Rappe, A. K.; Casewit, C. J.; Colwell, K. S.; Goddard, W. A.; Skiff, W. M. *J. Am. Chem. Soc.* **1992**, *114*, 10024–10035.
(62) Pitoňák, M.; Neogrády, P.; Hobza, P. *Phys. Chem. Chem. Phys.* **2010**, *12*, 1369–1378.
(63) Langner, K. M.; Sokalski, W. A.; Leszczyński, J. *J. Chem. Phys.* **2007**, *127*, 111102.